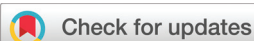


## PAPER



Cite this: *Polym. Chem.*, 2023, **14**, 5208

# Anti-inflammatory unimolecular micelles of redox-responsive hyperbranched polycurcumin amphiphiles with enhanced anti-inflammatory efficacy *in vitro* and *in vivo*†

Da Huang,<sup>a</sup> Qiang Tang,<sup>a</sup> Minglang Zou,<sup>a</sup> Yongming Wang,<sup>a</sup> Fang Luo,<sup>a,b</sup> Jinyi Mu,<sup>a</sup> Yuanzi Wu,<sup>a</sup> Zuquan Weng<sup>\*a,b</sup> and Zhenyu Lin<sup>†b</sup>

Inflammation is a critical immune response to various stimuli but can lead to diseases when uncontrolled. Commonly used anti-inflammatory drugs usually associated with side effects, natural products such as curcumin (CUR) have emerged as a promising alternative but suffer from low bioavailability. This study introduces a novel nanocarrier, amphiphilic hyperbranched polyprodrug (P(ACPP-co-CURMA)-b-POEGMA, PACE), designed to enhance the anti-inflammatory activity of CUR. PACE micelles, formed from a hydrophobic hyperbranched polyprodrug core and hydrophilic POEGMA corona, demonstrated remarkable stability, even upon dilution, and efficiently released CUR in response to the reductive intracellular environment. These micelles were biocompatible and effectively internalized by macrophages. In both *in vitro* and *in vivo* studies, PACE micelles demonstrated significant anti-inflammatory activity, reducing ROS levels, down-regulating pro-inflammatory cytokines, and alleviating inflammation. This work highlights the potential of PACE micelles as a promising platform for targeted and responsive anti-inflammatory therapy, with implications for treating inflammatory disorders.

Received 22nd September 2023,  
Accepted 12th November 2023

DOI: 10.1039/d3py01071f

rs.c.li/polymers

## Introduction

Inflammation constitutes a crucial defensive immune response elicited in response to a variety of extraneous stimuli, such as chemical irritants, pathogens, physical trauma, radiation, and burns. During the initial phase of inflammation, specialized immune cells are recruited to the site of infection or injury, subsequently releasing localized inflammatory mediators. This orchestrated response aims to clear the causative factors and facilitate tissue repair.<sup>1–3</sup> However, when inflammation becomes excessive or persists unabated, it can result in the accumulation of activated inflammatory cells in the connective tissues surrounding blood vessels. This chronic inflammation can lead to tissue damage and contribute to the development of various diseases including rheumatoid arthritis, inflammatory bowel diseases, atherosclerosis, asthma, and

cystic fibrosis.<sup>4–6</sup> Therefore, the timely implementation of anti-inflammatory therapies holds significant promise in the treatment and management of these ailments.

Clinically, the treatment of inflammatory diseases commonly relies on drugs including glucocorticoids (*e.g.*, hydrocortisone, prednisone, prednisolone) and non-steroidal anti-inflammatory drugs (*e.g.*, paracetamol, indomethacin, diclofenac, ibuprofen).<sup>7</sup> Despite their efficacy against various diseases, these medications are often accompanied by undesirable side effects, including cardiovascular toxicity and gastrointestinal damage.<sup>8,9</sup> Hence, there has been a growing interest in natural polyphenols as a novel class of anti-inflammatory agents due to their excellent biocompatibility. Numerous studies have documented the ability of polyphenols to exert anti-inflammatory effects by scavenging reactive oxygen species (ROS), modulating the activity of enzymes involved in inflammatory responses, and regulating the production of inflammatory mediators and cytokines, such as tumor necrosis factor- $\alpha$  (TNF- $\alpha$ ), interleukin 1 $\beta$  (IL-1 $\beta$ ), and prostaglandin E2 (PGE2).<sup>10–12</sup> Among these natural polyphenols, curcumin (CUR), derived from turmeric, stands out as a “Nature’s panacea” due to its multifaceted pharmacological properties, including antioxidative, anti-inflammatory, anti-angiogenic, and anti-cancer activities.<sup>13–15</sup> CUR has demonstrated anti-inflammatory efficacy in the treatment of various inflammatory

<sup>a</sup>College of Biological Science and Engineering, Fuzhou University, Fuzhou, Fujian 350108, China. E-mail: huangda@fzu.edu.cn, wengzq@fzu.edu.cn

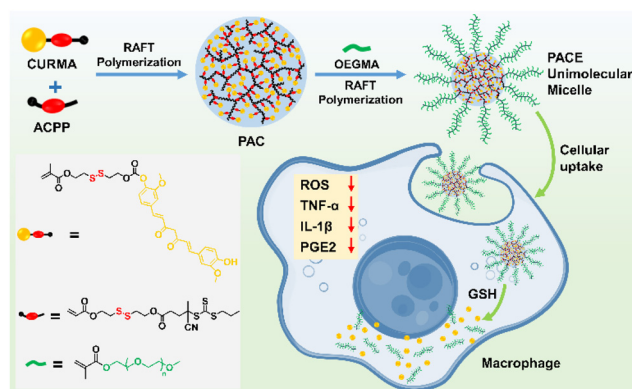
<sup>b</sup>Ministry of Education Key Laboratory for Analytical Science of Food Safety and Biology, Fujian Provincial Key Laboratory of Analysis and Detection for Food Safety, College of Chemistry, Fuzhou University, Fuzhou, Fujian 350108, China

†Electronic supplementary information (ESI) available: Materials and characterizations, synthesis of monomers, GPC traces of polymers, redox-responsive degradation of PACE. See DOI: <https://doi.org/10.1039/d3py01071f>

diseases, including Alzheimer's disease, Parkinson's disease, multiple sclerosis, colitis, and rheumatoid arthritis.<sup>16–18</sup> Importantly, as a naturally derived food product, CUR is relatively safe even at high doses of up to 12 grams per day in humans.<sup>19,20</sup> However, despite its immense potential, the clinical application of CUR has been significantly hampered by its poor water solubility and limited bioavailability.<sup>21</sup> Addressing these limitations could substantially enhance CUR's anti-inflammatory activity and its potential as an anti-inflammatory agent.

Recent research has unveiled a passive targeting effect in inflammatory tissues, akin to the enhanced permeation and retention effect observed in tumor tissues. Inflammatory tissues exhibit increased vascular permeability due to the loss of intercellular junctions between endothelial cells, triggered by hypoxia. Furthermore, the presence of various immune cell subsets, including neutrophils, monocytes/macrophages, T-cells, and dendritic cells, contributes to abnormal angiogenesis, further enhancing vascular permeability.<sup>22–24</sup> This distinctive characteristic allows macromolecular agents and nanoparticles to selectively accumulate in inflammatory tissues through leaky vessels. Consequently, the development of nanomedicines holds considerable promise for the treatment of inflammatory diseases. Moreover, the microenvironment of inflammatory tissues exhibits specific pathophysiological features, including lower pH values, elevated redox potential, and overexpression of enzymes (*e.g.*, neutrophil elastase, myeloperoxidase).<sup>25–27</sup> In this context, stimuli-responsive nanocarriers, such as liposomes, polymeric micelles, and vesicles, have been designed for the delivery of anti-inflammatory agents.<sup>4</sup> For instance, Liu *et al.* reported redox-responsive polymersomes that release indomethacin in response to inflammation, significantly ameliorating inflammatory responses induced by lipopolysaccharide (LPS) in macrophages.<sup>27</sup> Nevertheless, most of these nanocarriers are constructed *via* self-assembly of amphiphilic polymers, potentially suffering from instability upon dilution *in vivo*. In contrast, unimolecular micelles, composed of a highly branched hydrophobic core and a hydrophilic shell, have attracted attention due to their exceptional stability.<sup>28–32</sup> It is noteworthy that unimolecular micelles can be easily synthesized to incorporate multiple payloads through reversible addition–fragmentation chain transfer (RAFT) polymerization of different monomers, utilizing a multifunctional chain transfer agent in one or two steps.<sup>33–35</sup> Importantly, unimolecular micelles fabricated by this strategy load drugs by chemical conjugation *via* cleavable linkers. Compared to physical encapsulation, the conjugation approach mitigates the possibility of burst release and offers better control over drug release, because conjugated drugs can only be released once the linkers are cleaved in response to specific stimuli. Despite their potential, unimolecular micelles have yet to be explored as vehicles for the delivery of anti-inflammatory agents.

In this study, we present the development of redox-responsive unimolecular micelles based on hyperbranched polycurcumin amphiphiles (P(ACPP-*co*-CURMA)-*b*-POEGMA, PACE) as innovative macromolecular anti-inflammatory agents



**Scheme 1** Schematic Illustration of the preparation of PACE unimolecular micelles, their redox-responsive drug release and anti-inflammatory effect.

(Scheme 1). Initially, we designed and prepared a polymerizable CUR-based prodrug monomer containing a disulfide linker (CURMA). Then RAFT polymerization of the prodrug monomers with a multifunctional chain transfer agent (ACPP) yielded the hydrophobic hyperbranched polycurcumin core (P(ACPP-*co*-CURMA), PAC) of the unimolecular micelles. Subsequently, a hydrophilic shell poly(oligo(ethylene glycol) methacrylate) (POEGMA) was formed through polymerization of OEGMA on the surface of the hydrophobic core. This unique covalently interconnected amphiphilic core–shell structure existed as unimolecular micelles in aqueous solutions, maintaining their integrity even under conditions of dilution. The stability, redox-responsive cleavage and release of CUR, cellular uptake and cytocompatibility of the unimolecular micelles were investigated. Furthermore, anti-inflammatory activity of the unimolecular micelles was evaluated in LPS-treated RAW264.7 macrophages and zebrafish models.

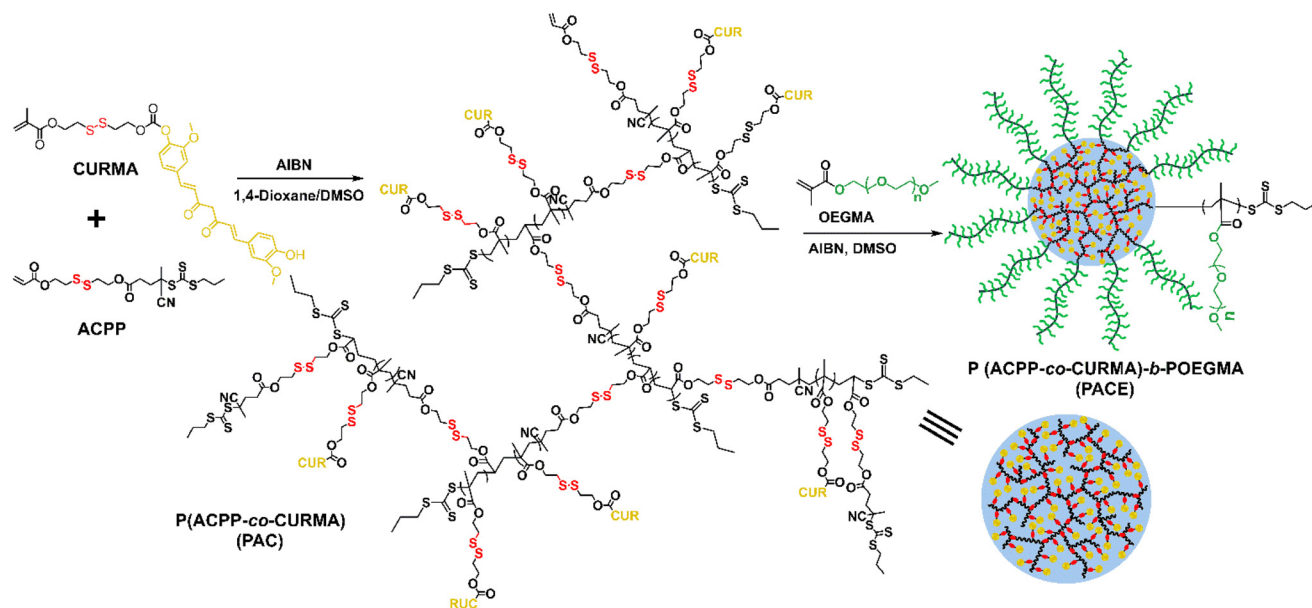
## Experimental section

### Synthesis of PAC

PAC was synthesized *via* RAFT polymerization of ACPD and CURMA as shown in Scheme 2. Briefly, CURMA (259 mg, 0.42 mmol), ACPD (19.64 mg, 0.042 mmol), and AIBN (1.37 mg, 0.0084 mmol) were charged into a round-bottom flask containing 1 mL of a mixed solvent consisting of DMSO and 1,4-dioxane (1 : 1, v/v). The mixture was subjected to three freeze–pump–thaw cycles to remove oxygen and was then placed in an oil bath thermostated at 90 °C to initiate polymerization. After 30 hours, the reaction was quenched by immersion in an ice-water bath. The resulting crude product was precipitated in excess diethyl ether for three times. The final product, a yellow solid powder, was obtained after vacuum drying (217 mg, yield: 78%).

### Synthesis of PACE

PACE was synthesized by RAFT polymerization of OEGMA using PAC as macroinitiators. PAC (50 mg), OEGMA (250 mg,



**Scheme 2** Synthetic route of the PACE amphiphilic hyperbranched polymer.

1.05 mmol), and AIBN (1.94 mg, 0.012 mmol) were placed in a round-bottom flask containing 1.5 mL of DMSO. After three freeze–pump–thaw cycles to eliminate oxygen, the flask was immersed in an oil bath maintained at 90 °C to initiate the polymerization. After 30 hours, the reaction was quenched in an ice-water bath. The crude product was precipitated in excess diethyl ether for three times, yielding a highly viscous jelly (191 mg, yield: 64%).

### Preparation of PACE unimolecular micelles

Unimolecular micelles composed of PACE were prepared using a solvent exchange method. Initially, PACE was dissolved in DMSO at a concentration of 20.0 mg mL<sup>-1</sup>. The solution was subsequently dialyzed against deionized water using a dialysis membrane with a molecular weight cutoff (MWCO) of 3500 Da. The dialysis buffer was refreshed every 4 hours. The resulting PACE unimolecular micelles solution was concentrated or diluted as needed for further experiments.

### Stability of PACE unimolecular micelles

Stability of the PACE unimolecular micelles was investigated by monitoring their size distributions by dynamic light scattering (DLS). Initially, the size distribution of PACE unimolecular micelles with a concentration of 1 mg mL<sup>-1</sup> was measured using a zetasizer. Then the solution was diluted to 0.5, 0.25, 0.1, 0.01 mg mL<sup>-1</sup> in sequence, and their size distributions were measured. To assess their responsiveness to redox, PACE unimolecular micelles with a concentration of 1 mg mL<sup>-1</sup> was incubated with 10 mM dithiothreitol (DTT) for 12 and 24 hours, followed by measurements of size distributions. At the end of the degradation experiment, the degradation products were observed by transmission electron microscopy (TEM) to verify their morphology and analyzed by high per-

formance liquid chromatography (HPLC) to affirm if intact CUR was released from the PACE unimolecular micelles.

### *In vitro* release of CUR from PACE unimolecular micelles

To measure drug loading content (DLC) of CUR, PACE was dissolved in DMSO at a concentration of 1 mg mL<sup>-1</sup>. Then UV absorbance of the solution at 420 nm (CUR) was measured, and the concentration of CUR was calculated using a standard curve. DLC was determined using the formula: DLC = (mass of CUR/mass of PACE) × 100%

The release of CUR from PACE unimolecular micelles was performed in phosphate-buffered saline (PBS) with varying DTT concentrations at 37 °C. A specified amount of PACE solution (1 mg mL<sup>-1</sup>) was placed inside a dialysis tubing (MWCO = 3500 Da) and immersed in 20 mL of pH 7.4 PBS medium containing different concentrations of DTT (10 μM and 10 mM) at 37 °C with shaking. At pre-determined time intervals, 2 mL of external medium was sampled and replaced with 2 mL of fresh medium. The CUR concentrations in the medium were determined by measuring UV absorbance at 420 nm using a microplate reader.

### Cellular uptake assay

All cell lines were obtained from the China Center for Type Culture Collection (Wuhan, China). RAW 264.7 macrophages were cultured in DMEM supplemented with 10% FBS and 1 wt% penicillin/streptomycin at 37 °C in a 5% CO<sub>2</sub> incubator. Subsequently, the cells were seeded onto glass-bottomed culture dishes at a density of 6 × 10<sup>4</sup> cells per well in 1 mL of medium. After 24 hours, the culture medium was replaced with 1 mL of fresh medium containing PACE, equivalent to 25 μg mL<sup>-1</sup> CUR. Following 1, 2, and 4 hours of incubation, the culture medium was aspirated, and the cells were gently

washed three times with cold PBS (2 mL, pH 7.4). The cells were then fixed using paraformaldehyde for 10 minutes. Following fixation, the cells were treated with  $1.00 \mu\text{g mL}^{-1}$  DAPI for 15 minutes to label the cell nuclei. Finally, the cells were washed three times with PBS and mounted on the culture dish for observation using confocal laser scanning microscopy (CLSM) with a FITC filter (excitation at 488 nm) to monitor the localization of PACE micelles within RAW 264.7 macrophages.

#### Cytotoxicity assay

The relative cytotoxicity of free CUR and PACE against RAW 264.7 macrophages or Human Skin Fibroblast (HSF) cells was assessed by CCK-8 assay. Cells were seeded into 96-well plates at a density of  $5 \times 10^3$  cells per well in 200  $\mu\text{L}$  medium. After 24 hours of incubation, the culture medium was removed, and the cells were treated with 200  $\mu\text{L}$  of medium containing serial dilutions of free CUR and PACE. Following 48 hours of incubation, the culture medium was aspirated, and 100  $\mu\text{L}$  of fresh medium and 10  $\mu\text{L}$  of CCK-8 were added to each well. After an additional 2 hours of incubation, the absorbance at 450 nm was measured using a microplate reader. The relative cell viability was calculated by comparing the absorbance of the treated wells to that of the wells without treatment.

#### Intracellular ROS imaging within RAW 264.7 macrophages

The intracellular ROS imaging assay was performed with slight modifications according to reported procedures.<sup>27</sup> RAW 264.7 macrophages were seeded onto glass-bottomed culture dishes at a density of  $6 \times 10^4$  cells per well in 1 mL of medium and were divided into four groups. Following a 24-hour incubation period, the culture media were refreshed with fresh media. Among the four groups, three sets of cells were exposed to LPS at a concentration of  $100 \text{ ng mL}^{-1}$  for a duration of 12 hours, while one set of cells was left untreated to serve as the control group. Following this, the three sets of LPS-treated cells were co-cultured with different treatments: PBS, free CUR, and PACE (equivalent to  $100 \mu\text{g mL}^{-1}$  CUR), respectively. After 24 hours of incubation, cells were treated with DCFH-DA and DAPI for 30 minutes to label ROS and nuclei, respectively. Subsequently, cells were observed using CLSM. The green fluorescence of ROS-activated 2',7'-dichlorofluorescein (DCF) was observed with excitation of 488 nm and emission of  $520 \pm 20$  nm. The blue fluorescence of DAPI within cell nuclei was observed using a 405 nm laser with an emission channel set to  $450 \pm 20$  nm.

#### Measurement of pro-inflammatory cytokines in RAW 264.7 macrophages

RAW 264.7 macrophages were seeded into 96-well plates at a density of  $1 \times 10^4$  cells per well in 200  $\mu\text{L}$  of medium and were divided into four groups. After 24 hours, the culture medium was replaced with fresh medium. Three sets of cells were treated with LPS ( $100 \text{ ng mL}^{-1}$ ) and subsequently exposed to PBS, free CUR, or PACE (equivalent to  $100 \mu\text{g mL}^{-1}$  CUR) for 24 hours, while one set of cells remained untreated as the control. After 24 hours, the levels of TNF- $\alpha$ , IL-1 $\beta$ , and PGE2 in

the culture media were determined using ELISA kits following the manufacturer's instructions.

#### In vivo ROS imaging within zebrafish

Zebrafish larvae (7 days post fertilization) were cultured in 200  $\mu\text{L}$  of culture medium in 96-well plates at 28  $^{\circ}\text{C}$  and were divided into four groups. After 24 hours of incubation, the culture medium was replaced with fresh medium. Three sets of larvae were incubated with LPS ( $20 \mu\text{g mL}^{-1}$ ) and subsequently exposed to PBS, free CUR, or PACE (equivalent to  $100 \mu\text{g mL}^{-1}$  CUR) for 24 hours, while one set of larvae remained untreated as the control. After 24 hours, the zebrafish larvae were incubated with  $20 \mu\text{g mL}^{-1}$  DCFH-DA solution for 1 hour to probe ROS. Stained larvae were then observed using a fluorescence microscope to evaluate the ROS levels *in vivo*.

#### Statistical analysis

Data were presented as mean  $\pm$  standard deviation (SD). Student's *t*-test was performed to compare the statistical difference between two groups, while one-way ANOVA was used for more groups. The star \* indicates the level of statistical significance  $p < 0.05$ . The star \*\* indicates the level of statistical significance  $p < 0.01$ . The star \*\*\* indicates the level of statistical significance  $p < 0.001$ . The plotting was performed using GraphPad Prism 8 software.

## Results and discussion

#### Synthesis of PACE

To obtain hyperbranched polymer *via* one-step radical polymerization, the use of a multifunctional RAFT chain transfer agent with a polymerizable functional group is essential, as branching occurs during the RAFT chain transfer agent itself gets involved in the polymerization. Hence, we firstly synthesized a multifunctional RAFT chain transfer agent ACPD and the polymerizable CUR prodrug CURMA using the synthetic routes shown in Scheme S1.† The successful synthesis of these compounds, along with all intermediate products, was confirmed by the  $^1\text{H}$  NMR spectra (Fig. S1–5†).

Subsequently, we synthesized amphiphilic hyperbranched polyprodrug PACE *via* a two-step RAFT polymerization process (Scheme 2). Initially, we synthesized the hyperbranched hydrophobic core PAC by RAFT polymerization of CURMA and ACPD. The  $^1\text{H}$  NMR spectrum of PAC is shown in Fig. 1A. The multiple peaks between 6.7 to 7.7 ppm correspond to the characteristic protons from the benzene ring in CUR moieties, with a signal at 9.71 ppm corresponding to the characteristic protons of hydroxyl in CUR moieties. The number-average molecular weight ( $M_n$ ) and weight-average molecular weight ( $M_w$ ) of PAC, determined by GPC, are 18.1 kDa and 23.5 kDa respectively, with a polydispersity of 1.30 (Fig. S6 and Table S1†), confirming the successful synthesis of hyperbranched polyprodrug PAC.

The second step involved the RAFT polymerization of OEGMA on the surface of the PAC core to grow hydrophilic

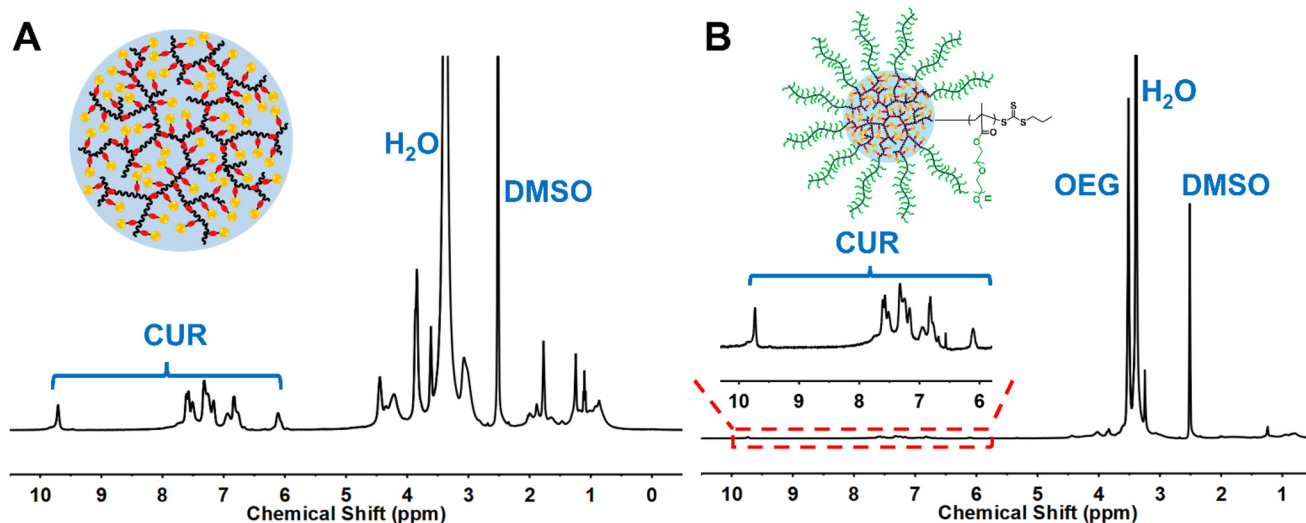


Fig. 1  $^1\text{H}$  NMR spectra of (A) PAC and (B) PACE in  $\text{DMSO}-d_6$ .

corona chains. As shown in Fig. 1B, the appearance of new resonance signals at 3.49 ppm attributed to POEGMA in the  $^1\text{H}$  NMR spectrum of PACE confirms the successful polymerization. The  $M_n$  and  $M_w$  of PACE, determined by GPC, are 148.9 kDa and 189.2 kDa respectively, with a polydispersity of 1.271 (Fig. S6 and Table S1†). These results confirm the successful synthesis of amphiphilic hyperbranched polydrug PACE.

The drug CUR content in PACE was determined to be approximately 5.8 wt% based on the UV-Vis absorbance of CUR using a calibration curve (Fig. S7†). Given that the CUR was conjugated to the hydrophobic core of the hyperbranched amphiphiles, the drug loading can be controlled by varying the ratio of the hydrophobic core and hydrophilic corona. However, this ratio should be balanced to ensure the colloidal stability of the resulted unimolecular micelles. It's worth mentioning that we tried to prepare PACE with higher CUR content, but precipitate was observed during the dialysis due to the aggregation of polymers. The results were in accordance with previous reports that the unimolecular micelles based on amphiphilic polydrug usually demonstrated drug loading content of 5–20 wt% depending on the hydrophilicity of drugs.<sup>33,34</sup>

### Preparation and characterization of PACE unimolecular micelles

As an amphiphilic polymer, PACE was expected to exist as unimolecular micelles in aqueous solutions by utilizing the hyperbranched PAC as the hydrophobic core and POEGMA multi-arms as the hydrophilic shell. However, the possibility of PACE forming multimolecular aggregates in aqueous solutions also existed. Therefore, we investigated the behavior of PACE in water using the conventional cosolvent approach (water and THF). The PACE was initially dissolved in THF ( $1.0 \text{ mg mL}^{-1}$ ), a solvent suitable for both PAC core and POEGMA shell. This

ensured that intermolecular aggregation of PACE could be ruled out. In Fig. 2A, the size of PACE in THF was approximately 43.82 nm (PDI = 0.228). Interestingly, the average hydrodynamic size of PACE in water measured by DLS was approximately 37.8 nm, with a uniform size distribution (PDI = 0.183), almost identical to that in THF. The slight decrease in size in water may be attributed to the hydrophobic PAC core contracting in the aqueous environment. TEM images indicated that PACE exhibited a monodisperse spherical morphology with an average diameter of approximately 28 nm, consistent with the DLS results (Fig. 2B). The zeta potential of PACE unimolecular micelles was measured at  $-14.8 \pm 1.3 \text{ mV}$ . The slightly negative surface charge of the PACE unimolecular micelles aligns with previous reports,<sup>33,34</sup> and can likely be ascribed to the absorption of negatively charged ions by the hydrated POEGMA corona. Notably, this negative surface charge, in conjunction with the hydrated POEGMA shell, are conducive to the colloidal stability of the micelles. These results suggest that PACE exists as structurally stable unimolecular micelles in aqueous solutions.

To confirm the exceptional stability of PACE unimolecular micelles upon dilution, we examined the concentration-dependent size of PACE by DLS. As shown in Fig. 2C and D, the particle size of PACE micelles remained almost constant as the aqueous solution was sequentially diluted from 1 to 0.5, 0.25, 0.1, and  $0.01 \text{ mg mL}^{-1}$ , further highlighting their structural stability. These results demonstrate that the hyperbranched polydrug PACE unimolecular micelles possess excellent stability, likely attributed to their covalently interconnected core-shell structure.

### *In vitro* redox-responsive degradation and drug release

The ability of nanoparticles to rapidly degrade and release payloads in response to the special environment at the lesion site is crucial for targeted drug delivery, as the accumulation of

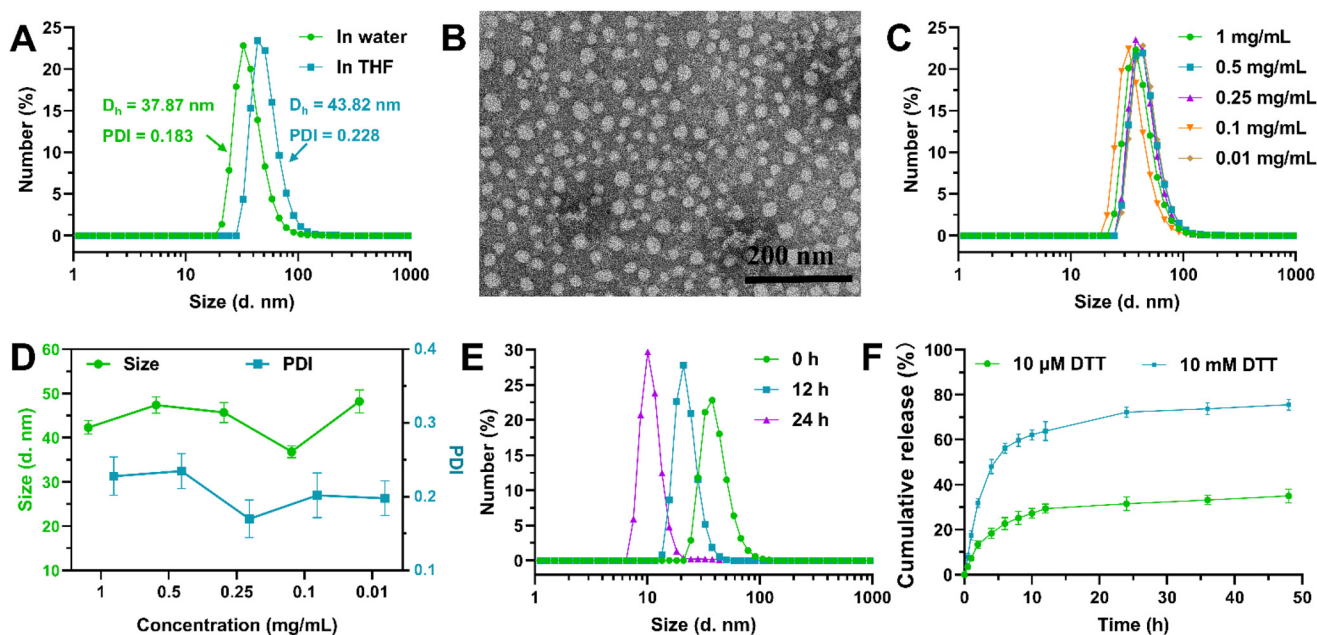


**Fig. 2** (A) Size distributions of PACE unimolecular micelles in water and THF. (B) TEM images of PACE unimolecular micelles. (C) Size distributions and (D) summarizations of sizes and PDIs of PACE unimolecular micelles in water at varying concentrations. (E) The variations of size distributions of PACE unimolecular micelles in response to 10 mM DTT over time. (F) Cumulative release profiles of CUR from PACE micelles after incubation with 10  $\mu$ M and 10 mM DTT.

nanoparticles in the body and nonspecific drug release can lead to severe side effects.<sup>6</sup> With disulfide bonds susceptible to cleavage in response to a redox milieu in the structure of PAC, the micelles could disintegrate in a highly reductive environment. Firstly, to study the redox-responsive degradation of PACE micelles, we treated the micelles with 10 mM DTT, which simulates the highly reductive environment in the cytoplasm. We measured the size of the micelles using DLS at specified time points. As shown in Fig. 2E, the size of the micelles gradually decreased from 41.24 nm to 10.39 nm within 24 hours. TEM image of the degradation products also displayed small fragments with sizes varying from a few nanometers to about 20 nm (Fig. S8<sup>†</sup>). These results indicated that PACE micelles could disintegrate due to the cleavage of disulfide bonds in a highly reductive environment.

CUR was attached to the hyperbranched PAC *via* disulfide bonds, which can be cleaved *via* glutathione (GSH)-mediated disulfide bond exchange, leading to the subsequent release of intact CUR through a self-immolative mechanism (Scheme S2<sup>†</sup>). Firstly, to verify if the PACE micelles can release pristine CUR in response to reductive stimulus, we analyzed the degradation products of PACE after 24 hours of incubation with 10 mM DTT by HPLC. As shown in Fig. S9<sup>†</sup>, a peak with the same retention time as free CUR was observed in the chromatogram of the degradation products, affirming that pristine CUR was released from the PACE unimolecular micelles.

Subsequently, to investigate the redox-responsive release behavior of PACE unimolecular micelles, *in vitro* release experiments were performed in PBS with 10  $\mu$ M DTT (simulating physiological conditions, such as bloodstream and the extra-

cellular matrix) and 10 mM DTT (simulating the intracellular inflammatory environment) at 37  $^{\circ}$ C, respectively. As shown in Fig. 2F, CUR was slowly released from PACE micelles in the presence of 10  $\mu$ M DTT, with only approximately 33% of CUR released within 48 hours. In contrast, approximately 65% of CUR was rapidly released from PACE micelles treated with 10 mM DTT within 12 hours. These results suggest that a higher concentration of DTT (representing a highly reductive environment) is more likely to break the disulfide bonds, resulting in a faster release of CUR from the micelles. It was reported that the inflammatory tissues exhibit elevated intracellular redox potential.<sup>27</sup> Therefore, the PACE micelles hold potential for use as a targeted macromolecular anti-inflammatory agent as they are relatively stable under physiological conditions but rapidly degrade and release CUR in an inflammatory environment.

#### Cellular uptake and cytotoxicity against macrophages

To confirm whether PACE unimolecular micelles can be internalized by immune cells at inflammatory sites, we visualized the cellular uptake of PACE micelles by RAW 264.7 macrophages using CLSM. As CUR exhibits intrinsic green fluorescence, we directly imaged the micelles without additional dye labeling. After predetermined incubation times, cell nuclei were stained with DAPI, and the cells were observed by CLSM. As shown in Fig. 3A, after 1 hour of culture with the micelles, green fluorescence from the micelles was clearly observed in the cytoplasm, indicating internalization *via* endocytosis. With increased incubation time, the green fluorescence became stronger and slowly diffused from the cytoplasm to the

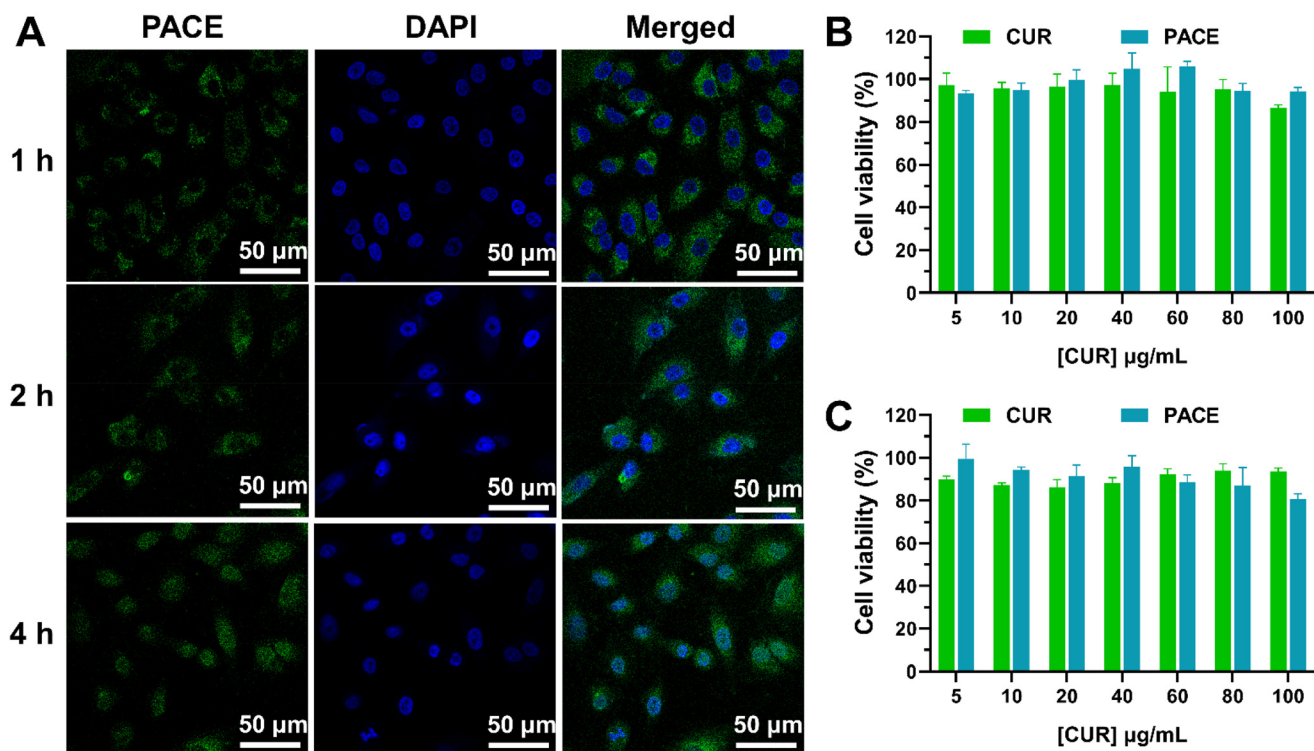


**Fig. 3** (A) CLSM images of RAW264.7 macrophages after incubation with PACE unimolecular micelles for 1, 2 and 4 hours. (Green: CUR; blue: nuclei labeled by DAPI). (B) Cytotoxicity of free CUR and PACE unimolecular micelles against (B) RAW264.7 macrophages and (C) HSF cells after 48 hours of incubation.

nucleus, suggesting increased cellular uptake of the micelles. These results confirm that PACE micelles can be effectively internalized by macrophages.

To evaluate the biocompatibility of PACE unimolecular micelles, we assessed the cytotoxicity of free CUR and PACE against RAW 264.7 macrophages and HSF cells using a CCK-8 assay. As shown in Fig. 3B and C after treatment with free CUR or PACE micelles at concentrations ranging from 5 to 100  $\mu\text{g mL}^{-1}$  for 48 hours, cell viability remained above 80%. This indicates that the formation of PACE micelles did not compromise the excellent biocompatibility of CUR, and PACE micelles were non-toxic to cells even at an equivalent CUR concentration of 100  $\mu\text{g mL}^{-1}$ . The cytocompatibility of PACE micelles is excellent.

#### ***In vitro* evaluation of anti-inflammatory effect of PACE micelles**

In the previous sections, we confirmed that the PACE unimolecular micelles degrade and release CUR in a redox-responsive manner and can be internalized by macrophages without inducing cytotoxicity. In the following part, anti-inflammatory effect of the PACE unimolecular micelles was further evaluated. It was reported that the oxidation stress is positively related to inflammation levels in inflammatory cells,<sup>36–38</sup> hence anti-inflammatory effect of the PACE unimolecular micelles was firstly investigated by observing the ROS level in LPS-treated RAW264.7 macrophages. As shown in Fig. 4A and B, the ROS levels in LPS-treated RAW 264.7 macrophages sig-

nificantly increased, indicating severe inflammation induced by LPS. Furthermore, incubation of LPS-treated cells with PACE micelles and free CUR both led to a significant decrease in fluorescence intensity compared to LPS-treated cells. Notably, the fluorescence intensity in cells treated with PACE micelles was lower than in CUR-treated cells. These results suggest that PACE micelles efficiently alleviate inflammation, possibly through the release of CUR mediated by intracellular elevated redox stress.

Inflammatory cells produce various pro-inflammatory cytokines, including IL-1 $\beta$ , TNF- $\alpha$ , and prostaglandin, which can further intensify inflammatory responses if left uncontrolled.<sup>5</sup> To further evaluate the anti-inflammatory activity of PACE micelles, we measured the levels of TNF- $\alpha$ , IL-1 $\beta$ , and PGE2 in LPS-treated RAW 264.7 macrophages after treatment with CUR or PACE micelles at different concentrations. As shown in Fig. 4C, the TNF- $\alpha$  levels in RAW 264.7 macrophages significantly increased after LPS treatment compared to untreated cells. However, incubation with free CUR or PACE micelles resulted in a significant decrease in TNF- $\alpha$  levels, with higher concentrations leading to greater reductions. Moreover, when comparing cells treated with equivalent CUR concentration, TNF- $\alpha$  levels in PACE micelle-treated cells were significantly lower than in CUR-treated cells, suggesting that PACE micelles exhibited superior anti-inflammatory effects. Similar results were observed for IL-1 $\beta$  and PGE2 measurements (Fig. 4D and E). These findings suggest that PACE micelles can effectively reduce inflammatory levels by

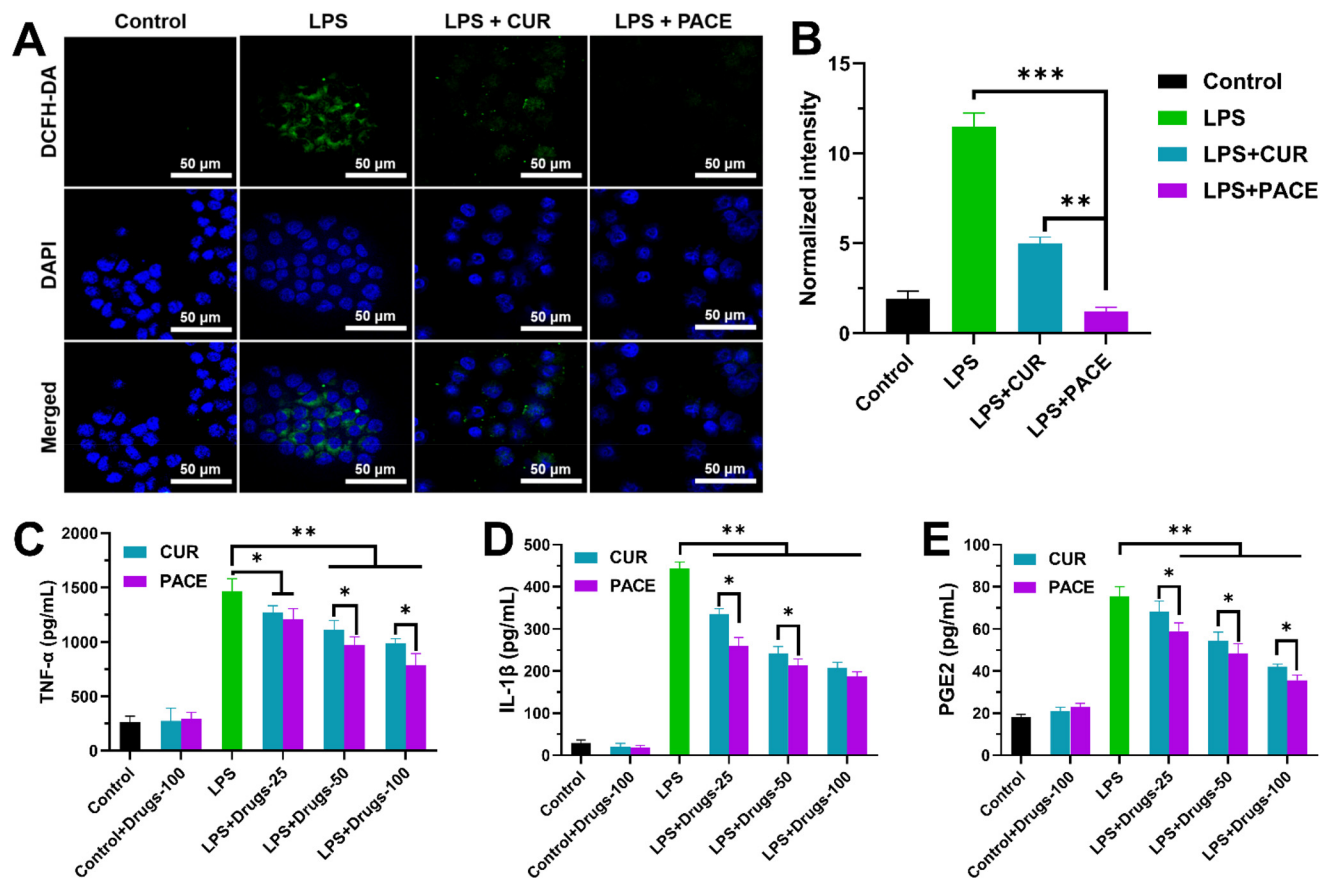


Fig. 4 (A) CLSM images of RAW 264.7 macrophages after different treatments (green: ROS probed by DCFH-DA; blue: nuclei labeled by DAPI). (B) Normalized fluorescence intensities of green channels quantified from CLSM results. The levels of pro-inflammatory cytokines (C) TNF- $\alpha$ , (D) IL-1 $\beta$ , (E) PGE2 in RAW 264.7 macrophages after different treatments (the 25, 50, 100 represent the concentrations of CUR with a unit of  $\mu\text{g mL}^{-1}$ ).

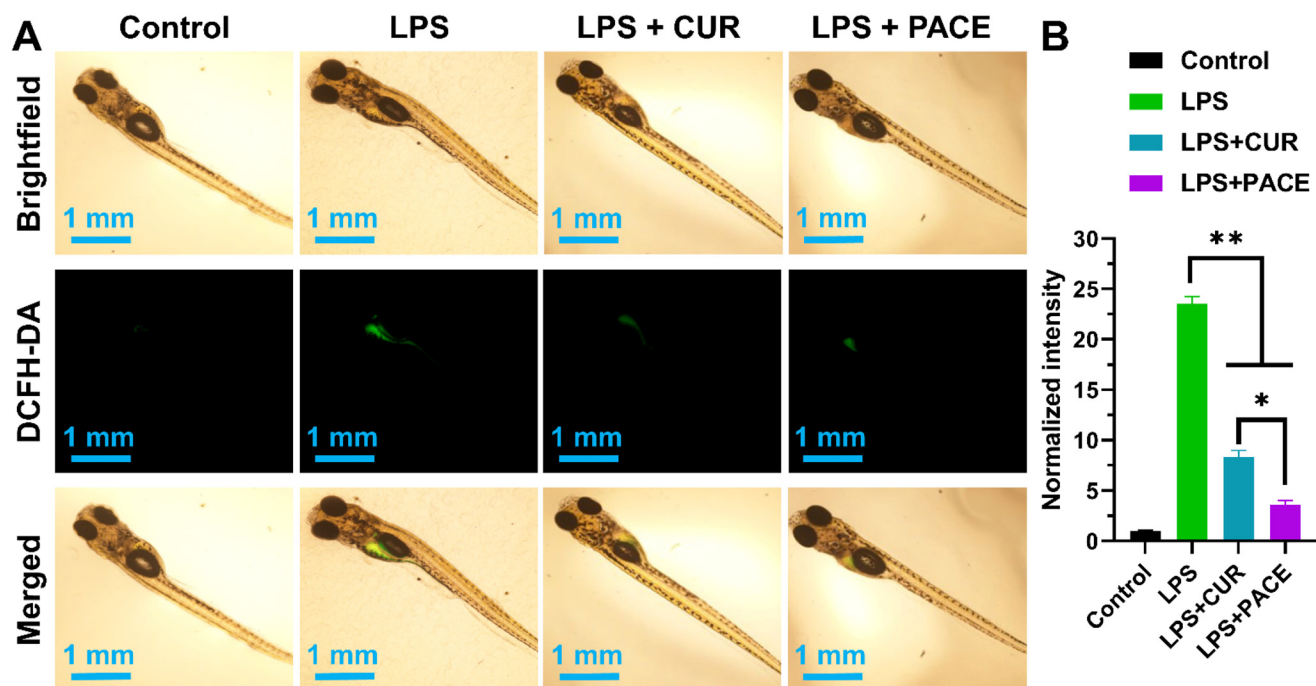


Fig. 5 (A) CLSM images of zebrafishes after different treatments (green: ROS probed by DCFH-DA). (B) Normalized fluorescence intensities of green channels quantified from CLSM results.

down-regulating pro-inflammatory cytokines. The enhanced anti-inflammatory activity of the PACE unimolecular micelles including their ability to reduce ROS and downregulate the levels of pro-inflammatory cytokines can be attributed to the increased bioavailability of CUR, facilitated by its improved solubility in aqueous solutions. While it is noteworthy that the degradation of PACE might deplete cellular GSH, the PACE unimolecular micelles still demonstrate superior ROS attenuation compared to free CUR. This suggests that the enhanced bioavailability of CUR adequately compensates for the consumption of endogenous antioxidants.

### *In vivo* evaluation of anti-inflammatory effect of PACE micelles

Encouraged by the *in vitro* results, we further assessed the anti-inflammatory activity of PACE micelles in zebrafish by monitoring ROS levels. Zebrafish, with strong similarities to humans in genetic makeup, has been widely used in biomedical research due to the advantages of strong reproductive ability, *in vitro* fertilization, ease of breeding, and high transparency of embryos and larvae.<sup>39,40</sup> As shown in Fig. 5A, the fluorescence intensity in zebrafish treated with LPS significantly increased, indicating an inflammatory response. However, incubation of LPS-treated zebrafish with PACE micelles and free CUR both resulted in a significant decrease in fluorescence intensity. The fluorescence intensity in zebrafish treated with PACE micelles was even lower than in CUR-treated zebrafish, as confirmed by quantitative analysis (Fig. 5B). These results suggest that PACE micelles demonstrated excellent anti-inflammatory activity *in vivo*.

## Conclusions

In conclusion, our study successfully synthesized amphiphilic hyperbranched polyprodrug PACE, designed to deliver the anti-inflammatory agent CUR in a targeted and controlled manner. PACE formed structurally stable unimolecular micelles, demonstrated excellent stability upon dilution, and exhibited redox-responsive degradation, releasing CUR efficiently in redox milieu. These micelles were effectively internalized by macrophages without inducing cytotoxicity, highlighting their biocompatibility. Furthermore, PACE micelles displayed remarkable anti-inflammatory properties, both *in vitro* and *in vivo*, as evidenced by the reduction in ROS levels, down-regulation of pro-inflammatory cytokines, and significant alleviation of inflammation. Collectively, our findings support the potential utility of PACE micelles as a promising platform for targeted and responsive anti-inflammatory therapy, with implications for the treatment of inflammatory disorders.

## Author contributions

Da Huang: conceptualization, methodology, investigation, writing – original draft & review & editing; Qiang Tang: methodology, investigation, validation; Minglang Zou: method-

ology, investigation; Yongming Wang: methodology, validation; Fang Luo: methodology; Jinyi Mu: investigation; Yuanzi Wu: formal analysis; Zuquan Weng: supervision, writing – review & editing; Zhenyu Lin: resources.

## Conflicts of interest

There are no conflicts to declare.

## Acknowledgements

The authors acknowledge the financial support from the National Natural Science Foundation of China (81971837), and the Natural Science Foundation of Fujian Province (2023J01410).

## References

- 1 M. E. Kotas and R. Medzhitov, *Cell*, 2015, **160**, 816–827.
- 2 G. M. Slavich, *Brain, Behav., Immun.*, 2015, **45**, 13–14.
- 3 Z. Tu, Y. Zhong, H. Hu, D. Shao, R. Haag, M. Schirner, J. Lee, B. Sullenger and K. W. Leong, *Nat. Rev. Mater.*, 2022, **7**, 557–574.
- 4 Y. Dou, C. Li, L. Li, J. Guo and J. Zhang, *J. Controlled Release*, 2020, **327**, 641–666.
- 5 W. He, N. Kapate, C. W. Shields and S. Mitragotri, *Adv. Drug Delivery Rev.*, 2020, **165–166**, 15–40.
- 6 M. Zhang, W. Hu, C. Cai, Y. Wu, J. Li and S. Dong, *Mater. Today Bio*, 2022, **14**, 100223.
- 7 G. Mahesh, K. A. Kumar and P. Reddanna, *J. Inflammation Res.*, 2021, **14**, 253–263.
- 8 B. Cryer, *Curr. Opin. Gastroenterol.*, 2001, **17**, 503–512.
- 9 S. Bindu, S. Mazumder and U. Bandyopadhyay, *Biochem. Pharmacol.*, 2020, **180**, 114147.
- 10 M. Sobhani, M. H. Farzaei, S. Kiani and R. Khodarahmi, *Food Rev. Int.*, 2021, **37**, 759–811.
- 11 H. Khan, A. Sureda, T. Belwal, S. Çetinkaya, İ. Süntar, S. Tejada, H. P. Devkota, H. Ullah and M. Aschner, *Autoimmun. Rev.*, 2019, **18**, 647–657.
- 12 T. Behl, K. Mehta, A. Sehgal, S. Singh, N. Sharma, A. Ahmadi, S. Arora and S. Bungau, *Crit. Rev. Food Sci.*, 2022, **62**, 5372–5393.
- 13 M. E. Egan, M. Pearson, S. A. Weiner, V. Rajendran, D. Rubin, J. Glockner-Pagel, S. Canny, K. Du, G. L. Lukacs and M. J. Caplan, *Science*, 2004, **304**, 600–602.
- 14 S. Ghosh, S. Banerjee and P. C. Sil, *Food Chem. Toxicol.*, 2015, **83**, 111–124.
- 15 S. Prasad, S. C. Gupta, A. K. Tyagi and B. B. Aggarwal, *Biotechnol. Adv.*, 2014, **32**, 1053–1064.
- 16 Q. Wang, C. Ye, S. Sun, R. Li, X. Shi, S. Wang, X. Zeng, N. Kuang, Y. Liu, Q. Shi and R. Liu, *Int. Immunopharmacol.*, 2019, **72**, 292–300.
- 17 K. Shimizu, M. Funamoto, Y. Sunagawa, S. Shimizu, Y. Katanasaka, Y. Miyazaki, H. Wada, K. Hasegawa and T. Morimoto, *Eur. Cardiol. Rev.*, 2019, **14**, 117–122.

- 18 C. Xu, S. Chen, C. Chen, Y. Ming, J. Du, J. Mu, F. Luo, D. Huang, N. Wang, Z. Lin and Z. Weng, *Int. J. Pharm.*, 2022, **623**, 121884.
- 19 L. Lv, Y. Shen, M. Li, X. Xu, M. Li, S. Guo and S. Huang, *J. Biomed. Nanotechnol.*, 2014, **10**, 324–335.
- 20 L. Cheng, C. H. Hsu, J. K. Lin, M. M. Hsu, Y. F. Ho, T. S. Shen, J. Y. Ko, J. T. Lin, B. R. Lin, W. Ming-Shiang, H. S. Yu, S. H. Jee, G. S. Chen, T. M. Chen, C. A. Chen, M. K. Lai, Y. S. Pu, M. H. Pan, Y. J. Wang, C. C. Tsai and C. Y. Hsieh, *Anticancer Res.*, 2001, **21**, 2895–2900.
- 21 P. Anand, A. B. Kunnumakkara, R. A. Newman and B. B. Aggarwal, *Mol. Pharmaceutics*, 2007, **4**, 807–818.
- 22 F. Yuan, L.-d. Quan, L. Cui, S. R. Goldring and D. Wang, *Adv. Drug Delivery Rev.*, 2012, **64**, 1205–1219.
- 23 B. Axelsson, *Adv. Drug Delivery Rev.*, 1989, **3**, 391–404.
- 24 X. Zhou, X. Cao, H. Tu, Z.-R. Zhang and L. Deng, *Mol. Pharmaceutics*, 2019, **16**, 1397–1405.
- 25 M. Huo, J. Yuan, L. Tao and Y. Wei, *Polym. Chem.*, 2014, **5**, 1519–1528.
- 26 S. Mingchen, A. K. John, K. Hoda and P. F. Mitchell, *J. Pharmacol. Exp. Ther.*, 2004, **308**, 307.
- 27 J. Tan, Z. Deng, G. Liu, J. Hu and S. Liu, *Biomaterials*, 2018, **178**, 608–619.
- 28 X. Fan, Z. Li and X. J. Loh, *Polym. Chem.*, 2016, **7**, 5898–5919.
- 29 F. Qiu, Y. Huang and X. Zhu, *Macromol. Chem. Phys.*, 2016, **217**, 266–283.
- 30 C. Porsch, Y. Zhang, M. I. Montanez, J. M. Malho, M. A. Kostianen, A. M. Nystrom and E. Malmstrom, *Biomacromolecules*, 2015, **16**, 2872–2883.
- 31 C. Yang, S. Huang, X. Wang and M. Wang, *Polym. Chem.*, 2016, **7**, 7455–7468.
- 32 X. Fan, X. Wang, M. Cao, C. Wang, Z. Hu, Y.-L. Wu, Z. Li and X. J. Loh, *Polym. Chem.*, 2017, **8**, 5611–5620.
- 33 P. Sun, N. Wang, X. Jin and X. Zhu, *ACS Appl. Mater. Interfaces*, 2017, **9**, 36675–36687.
- 34 X. Hu, G. Liu, Y. Li, X. Wang and S. Liu, *J. Am. Chem. Soc.*, 2015, **137**, 362–368.
- 35 C. Zhang, Y. Zhou, Q. Liu, S. Li, S. Perrier and Y. Zhao, *Macromolecules*, 2011, **44**, 2034–2049.
- 36 M. M. Pomacu, M. D. Trașcă, V. Pădureanu, A. M. Bugă, A. M. Andrei, E. C. Stănciulescu, I. M. Baniță, D. Rădulescu and C. G. Pisoschi, *Exp. Ther. Med.*, 2021, **21**, 602.
- 37 S. Kumar, I. M. Adjei, S. B. Brown, O. Liseth and B. Sharma, *Biomaterials*, 2019, **224**, 119467.
- 38 A. Huguet-Casquero, Y. Xu, E. Gainza, J. L. Pedraz and A. Beloqui, *Int. J. Pharm.*, 2020, **586**, 119515.
- 39 P. Zhang, X.-f. Jiang, X. Nie, Y. Huang, F. Zeng, X. Xia and S. Wu, *Biomaterials*, 2016, **80**, 46–56.
- 40 F. Luo, S. Li, L. Cui, Y. Zu, Y. Chen, D. Huang, Z. Weng and Z. Lin, *Nanoscale*, 2021, **13**, 14297–14303.